Simulation of spin-torque diode microwave detectors

Article *in* The European Physical Journal Applied Physics · January 2015

DOI: 10.1051/epjap/2014140451

Xichao Zhang
The University of Hong Kong

Eur. Phys. J. Appl. Phys. (2015) 69: 10603
DOI: 10.1051/epjap/2014140451

The European Physical Journal
Applied Physics

Regular Article

Simulation of spin-torque diode microwave detectors

Chong Long Cao[1], Yan Zhou[2,a], Xi Chao Zhang[2], Yu Mao Wu[3], and Philip W.T. Pong[1,b]

[1] Department of Electrical and Electronic Engineering, The University of Hong Kong, Hong Kong
[2] Department of Physics, The University of Hong Kong, Hong Kong
[3] Key Laboratory for Information Science of Electromagnetic Waves (MoE), School of Information Science and Technology, Fudan University, Shanghai 200433, P.R. China

Received: 14 November 2014 / Received in final form: 7 December 2014 / Accepted: 10 December 2014

Abstract. Spin-torque microwave detectors (STMD) provide a novel means of measuring the radio-frequency signals. We discuss the influence of dimensional parameters and direct current (DC) bias current on the performance of an STMD. We reveal that the performance of an STMD does not always improve with the current density. We also discuss the influence of the direction of the fixed-layer polarization. The results can be used for the optimization of an STMD.

1 Introduction

Spin-transfer torque (STT) effect provides a method of manipulating magnetization in nano-scale objects which can be modeled by the Landau-Lifshitz-Gilbert-Slonczewski (LLGS) equation [1]. Due to the STT effect, the angular magnetic momentum can be transferred from the fixed layer of a magnetic tunnel junction (MTJ) to the free layer by the polarized current, giving rise to the microwave dynamics of magnetization in the free layer. This effect can be used for radio frequency generators [2]; however, the inverse effect can also be useful: by injecting microwave current to the MTJ, the resonance oscillation of the junction resistance can mix with the oscillation of the input microwave current and produce an output DC voltage across the junction. This inverse effect leads to the so-called spin torque diode effect and was first demonstrated experimentally in 2005 [3] and discussed theoretically [4,5]. The devices that utilize this effect are called the spin torque microwave detectors (STMDs). STMD is of great interest because it realizes the measurement of radio-frequency signal by a nano-scale detector, which has wide application in telecommunication circuits. The performance of an STMD can be characterized by measuring its output DC voltage while passing high-frequency current through the MTJ simultaneously [3]. From the point of view of application, the most important goal is to increase the output DC voltage of an STMD. Recently, Skowronski et al. reported the voltage-tuned resonance of STMDs exhibited an effect on the output voltage performance [6]. The rest of this article is arranged as follows: in Section 2, we present the theoretical modeling of the STMD; in Section 3, we carry out simulations to study the performance of the STMD under different physical parameters and we analyze the influence of the bias DC current and dimensional parameter (the radius of the tri-layer structure in Fig. 1a) of the STMD on the output voltage; in Section 4, we summarize the main elements that has influence on the performance of STMDs, revealing the nonlinear dependence of the output voltage on the DC current.

2 Modeling of spin torque microwave detectors

As shown in Figure 1a, the STMD is a three-layer system, consisting of a thick magnetically fixed layer, nonmagnetic spacer layer and a thin free (sensing) layer. The circuit of STMD used in this work is shown in Figure 1b. By solving the LLGS equation numerically [1,7], we can find the time-evolution of the free-layer magnetization $\hat{m}$:

$$\frac{\mathrm{d}\hat{m}}{\mathrm{d}t} = -|\gamma|\hat{m}\times\mathbf{H}_{\mathrm{eff}} + \alpha\hat{m}\times\frac{\mathrm{d}\hat{m}}{\mathrm{d}t} + |\gamma|\frac{\eta(I_{\mathrm{dc}}+I_{\mathrm{ac}})}{2\mu_0 M_{\mathrm{S}} e V_f}\hat{m}\times(\hat{m}\times\hat{M}). \quad (1)$$

The three terms on the right hand of the equation are the precession term, the damping term and the spin-torque term respectively, where $\hat{m}$ is the unit vector along the magnetization of the free layer, $\hat{M}$ is the unit vector along the magnetization of the fixed layer, γ is the gyromagnetic ratio, α is the damping coefficient, μ_0 is the magnetic vacuum permeability, η is the spin transfer efficiency, M_{S} is

---

[a] e-mail: yanzhou@hku.hk
[b] e-mail: ppong@eee.hku.hk

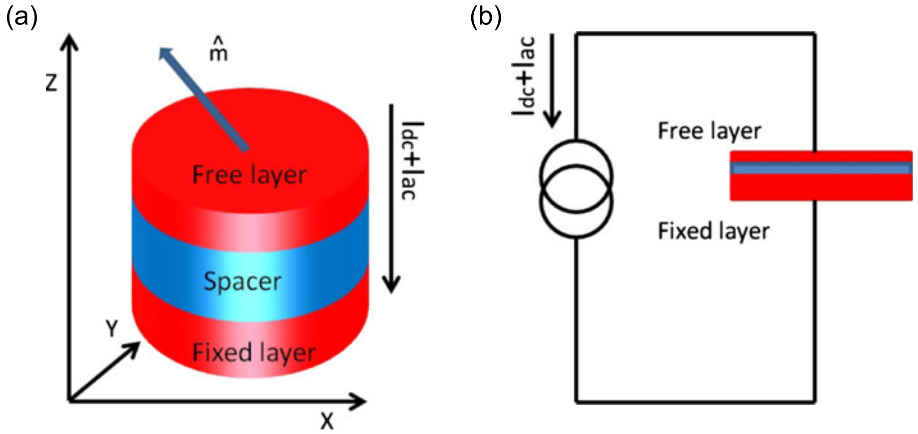

Fig. 1. (a) Schematics of the STMD model: $I_{\rm dc}$ and $I_{\rm ac}$ are the input DC current and radio-frequency current respectively, $\hat{m}$ is the unit vector of the free-layer magnetization. (b) Scheme of the circuit for measuring the radio-frequency signal.

the free-layer saturation magnetization, and V_f stands for the volume of the free layer. $\mathbf{H}_{\rm eff} = H_{\rm app}\hat{e}_x + H_k(\hat{m}\cdot\hat{e}_x)\hat{e}_x - H_d(\hat{m}\cdot\hat{e}_z)\hat{e}_z$ is the effective magnetic field acting on the free layer, which includes the applied magnetic field $H_{\rm app}$, the uniaxial magnetic anisotropy field H_k, and the out-of-plane demagnetization field H_d. $\hat{e}_x$ and $\hat{e}_z$ are the unit vectors along X (in-plane easy-axis) and Z (out-of-plane) respectively. We assume the following standard equation to describe the dependence of the resistance R of the STMD on the angle between the magnetization of fixed and free layer at time t:

$$R(t) = \frac{R_\perp}{1 + P^2\cos(\psi(t))}, \tag{2}$$

where P is the spin-polarization of current, $\psi(t)$ is the angle between the magnetization of the fixed layer and the free layer. $R_\perp$ is the resistance in the perpendicular magnetic state ($\psi(t) = \pi/2$) respectively.

We assume a DC bias current $I_{\rm dc}$ and a radio frequency AC current $I_{\rm ac}$ (Fig. 1b) are applied to the STMD simultaneously. As shown in Figure 1b, the total current flowing through the STMD is the summation of the DC current and AC current, $I_{\rm STMD} = I_{\rm dc} + I_{\rm ac}$. $I_{\rm ac}$ is the radio-frequency signal that needed to be measured and the bias DC current $I_{\rm dc}$ is used to tune the output voltage generated by a specified radio-frequency signal $I_{\rm ac}$. The output DC voltage across the STMD can be calculated simply using the Ohms law: $V_{\rm output} = \langle I_{\rm STMD} \times R(t)\rangle$, where $\langle\ \rangle$ denotes average over the integrated period.

3 Simulation results

The following parameters are adopted in our simulation [4,8–11]: $\alpha = 0.01$, $\gamma = 1.76 \times 10^{11}$ Hz/T, $\eta = 0.35$, $H_{\rm app} = 0.2$ T, $H_d = 0.75$ T, $P = 0.7$, $R_\perp = 1000\ \Omega$. The anisotropy field of the free layer of the STMD H_k is kept at zero.

The output voltage is determined by the input current and the resistance. From equation (2), the angle between the fixed layer and free layer plays an critical role in the resistance of the STMD. From equation (1), we can see that the time dependence of the angle $\psi(t)$ is determined by the spin torque term of the LLGS equation. First, we discuss the influence of the bias DC current and the dimensional parameter (radius in the present work) to improve the output voltage of the STMD. Figure 2 shows the macro-spin simulation results for perpendicular polarized current. In Figure 2a, we show the dependence of the output voltage on the bias DC current. The output voltage does not increases with the bias current monotonously under the given parameters. The output voltage first increases with the bias DC current and reaches the maximum at around 0.14 mA. This is because of the nonlinear property of the spin torque dependence of the LLGS equation [12]. For more detailed information, we plot the trajectory of the magnetization unit vector at points A and B respectively in the inset. We can see that the trajectory at point B is closer to the plane than the trajectories at points A and B, which means that point B has the maximum resistance. This explains the reason the output voltage reaches the maximum at point B. In Figure 2b, we performed a simulation to analyze the dependence of the output voltage on the radius when $I_{\rm dc} = 0.2$ mA. We can see that the output voltage improves with the radius of the STMD. This is because when the bias DC current becomes larger than 0.14 mA, the output voltage actually decreases with the density of DC current (Fig. 2a). It is interesting because the spin-torque is actually decreasing with the radius of the STMD. In the inset of Figure 2b, we plot the trajectory of the magnetization unit vector at points D and E respectively. The inset clearly shows that the resistance at point E is larger than that at point D. The detailed nonlinear dependence can be shown more intuitively in Figure 3. The dotted lines with fixed radius and DC current show similar results compared to Figure 2.

Besides the bias DC current and the radius, the angle between the fixed layer and the plane may also play an important role in the performance of the STMD. We performed the macrospin simulation to analyze the angular

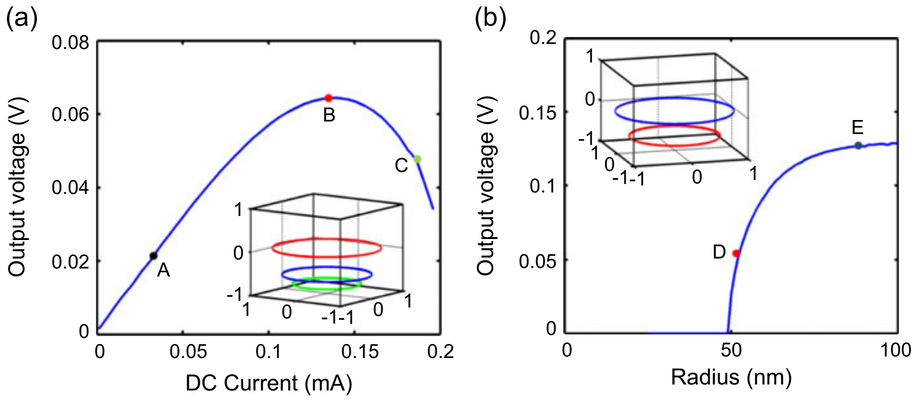

Fig. 2. (a) DC current dependence of the output voltage (radius $r = 50$ nm; saturation magnetization $M_\mathrm{S} = 0.8\ \mu$; applied field $H_\mathrm{app} = 0.2$ T alone X axis). Inset: the trajectory of the magnetization unit vector at points A (black), B (red) and C (green), respectively. (b) Radius dependence of the output voltage when the input DC current $I_\mathrm{dc} = 0.2$ mA. Inset: the trajectory of the magnetization unit vector at points D (red) and E (blue) respectively.

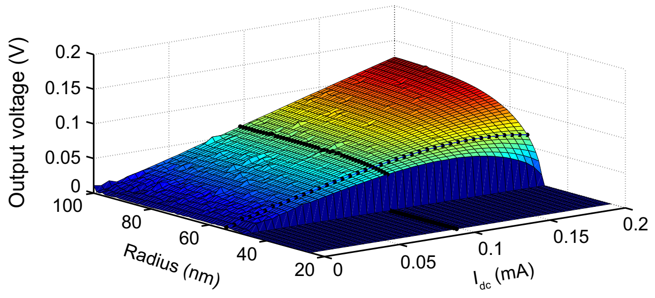

Fig. 3. The influence of radius and DC current on the output voltage, radius $\in [25, 100]$ nm, DC bias current $I_\mathrm{dc} \in [0, 0.2]$ mA. The two black dotted lines represent the voltage dependence on the DC current with radius = 50 nm and the voltage dependence on the radius with the DC current $I_\mathrm{dc} = 0.75$ mA respectively.

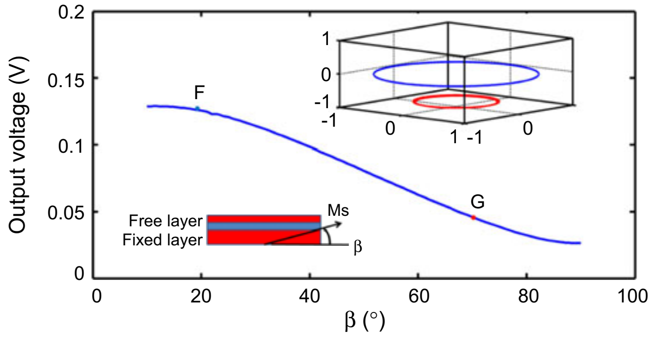

Fig. 4. The angular dependence of the output voltage, β is the angle between the fixed layer and plane (bottom left inset). $\beta \in [10°, 90°]$. Top right inset: the trajectory of the magnetization unit vector at points F (blue) and G (red).

dependence of the output voltage, and the result is shown in Figure 4. It is clearly shown that the output voltage decreases with β monotonously. The top right inset of

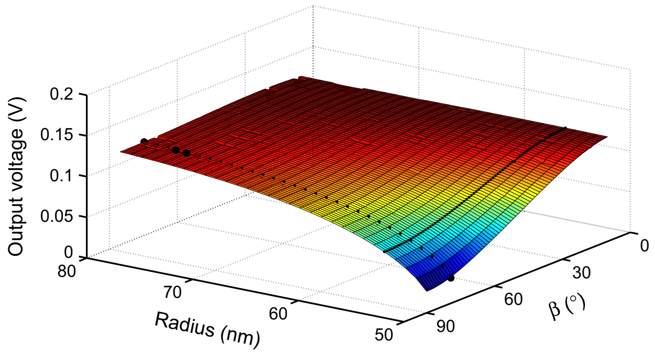

Fig. 5. The influence of the radius and β on the output voltage, radius $\in [50, 80]$ nm, $\beta \in [10°, 90°]$. The two black dotted lines represent the voltage dependence on the angle β with a radius of 55 nm and the voltage dependence on the radius while the angle $\beta = 80°$ respectively.

Figure 4 plots the trajectory of the magnetization unit vector at points F and G. We can see that the precession angle contributes to the resistance and hence the output voltage. Figure 5 shows the combined effects of the fixed-layer angle β and the radius on the output voltage. From Figure 5, we can see that the nonlinear angular dependence of the output voltage becomes smaller when the radius becomes larger. The dotted line with fixed radius shows similar angular dependence compared to Figure 4 and the dotted line with fixed β shows that the output voltage increases with radius for $\beta = 80°$, which agrees with the result in Figure 2b.

4 Conclusions

In summary, we have analyzed the influence of the bias DC current and dimensional parameter (radius) of the STMD on the output voltage. It is revealed that for perpendicular polarized current, the output voltage does not always increase with the input current density. We also have studied the influences of the polarization direction of current on the output voltage. The results provide useful information for optimizing the design parameters of an STMD in application.

This work is supported in part by the Seed Funding Program for Basic Research and Small Project Funding Program from the University of Hong Kong, ITF Tier 3 funding (ITS/112/12 and ITS/171/13), RGC-GRF under grant (HKU 17210014), RGC-GRF grant (HKU 704911P), University Grants Committee of Hong Kong (Contract No. AoE/P-04/08), the talent recruitment (Grant No. IDH1207001) by Fudan University, NSFC (Grant No. 61401103) and Natural Science Foundation of Shanghai government (Grant No. 14ZR1402400).

References

1. J.C. Slonczewski, J. Magn. Magn. Mater. **159**, 1 (1996)
2. Y. Zhou, J. Persson, S. Bonetti, J. Åkerman, Appl. Phys. Lett. **92**, 092505 (2008)
3. A. Tulapurkar, Y. Suzuki, A. Fukushima, H. Kubota, H. Maehara, K. Tsunekawa, D. Djayaprawira, N. Watanabe, S. Yuasa, Nature **438**, 339 (2005)
4. O.V. Prokopenko, E. Bankowski, T. Meitzler, V.S. Tiberkevich, A.N. Slavin, IEEE Trans. Magn. **48**, 3807 (2012)
5. O.V. Prokopenko, I.N. Krivorotov, E. Bankowski, T. Meitzler, S. Jaroch, V.S. Tiberkevich, A.N. Slavin, J. Appl. Phys. **111**, 123904 (2012)
6. W. Skowronski, M. Frankowski, J. Wrona, T. Stobiecki, P. Ogrodnik, J. Barnas, Appl. Phys. Lett. **105**, 072409 (2014)
7. L. Berger, Phys. Rev. B **54**, 9353 (1996)
8. J. Grollier, V. Cros, A. Fert, Phys. Rev. B **73**, 060409(R) (2006)
9. S.I. Kiselev, J.C. Sankey, I.N. Krivorotov, N.C. Emley, R.J. Schoelkopf, R.A. Buhrman, D.C. Ralph, Nature **425**, 380 (2003)
10. J. Xiao, A. Zangwill, M.D. Stiles, Phys. Rev. B **72**, 014446 (2005)
11. H. Xi, Z. Lin, A.M. Wilomowski, J. Magn. Magn. Mater. **296**, 32 (2006)
12. A.N. Slavin, V.S. Tiberkevich, IEEE Trans. Magn. **45**, 1875 (2009)